Improved shape for multi-surface blends

Kęstutis Karčiauskas[a] and Jörg Peters[b]
[a] Vilnius University [b] University of Florida

Abstract

For many design applications, where multiple primary surface pieces meet, the distribution of curvature is more important than formally achieving exact curvature continuity. For parametric spline surfaces, when constructing a multi-sided surface cap, we demonstrate a strong link between the uniform variation of the re-parameterization between (boundary) data of the joining pieces and a desirable distribution of curvature. We illustrate this interdependence between parameterization quality and surface quality by developing a G^1 bi-quintic surface cap consisting of n pieces that smoothly fills holes in a piecewise bi-cubic tensor-product spline complex. These bi-5 surface caps have arguably better shape than higher-degree, formally curvature continuous alternatives.

1. Introduction

Mathematically, since a given surface may be arbitrarily re-parameterized, the differential-geometric properties of surfaces do not depend on the choice of parameterization. In practice, in particular in the CAD context of a low-degree spline representations joining multiple primary surfaces via a multi-sided cap, we observe a strong correlation between the layout of parameter lines and the quality of the resulting surface. Varying the metric, as represented by the reparameterization, as uniformly as possible from the regular tensor-product spline setup along the boundary of the cap to its irregular, star-like center, appears to be crucial for good curvature distribution. Here our measure of quality is that the curvatures present in the primary surfaces along the boundaries of the surface cap average out in the cap without introducing unnecessary oscillations in the highlight lines.

The importance of a uniform layout of parameter lines in constructive algorithms can partly be explained by the strategy of setting degrees of freedom. Coefficients not already determined by formal smoothness constraints, are, in the absence of other constraints, set by minimizing functionals that combine the partial derivatives of the surface. The more gently this metric transitions from the standard tensor-product layout ($n = 4$) at the border to the meeting of $n \neq 4$ patches at the center, the better such functionals address the geometric properties of the resulting surface cap.

The contribution of this paper is two-fold. First, we document the interplay of parameterization and shape, and point out the value of reparameterizing all boundary data including the first derivative. Second, we present a surface construction of

moderate degree bi-5 with n patches to cap a tensor-product bi-cubic spline complex where n spline patches join. The visual, highlight line and even curvature quality of these caps is comparable and, at times, superior to more complex curvature continuous constructions, see Fig. 1. Where $n = 3$ pieces come together, Theorem 1 establishes that symmetric G^1 caps of any degree are automatically curvature continuous at their central irregular point.

This new result is part of a series of practical algorithms by the authors (see e.g. [KP09, KP13, KP14]) that explore the non-linear problem of surface construction with good shape – towards a better understanding of the mathematical properties that capture and optimize surface shape. Our approach is guided by testing against an *obstacle course of hard synthetic input data* [KP15] that are designed to expose the shortcomings of the existing methods.

Overview. Section 2 reviews comparable surface constructions. Section 3 formulates the surface blending problem. Section 4 explains the construction in the generic case when $n > 4$ and Section 5 discusses the decisions that lead to the construction. This section also compares the new construction to the G^2 constructions [LS08, KP13]. Section 6 focuses on the important special case $n = 3$.

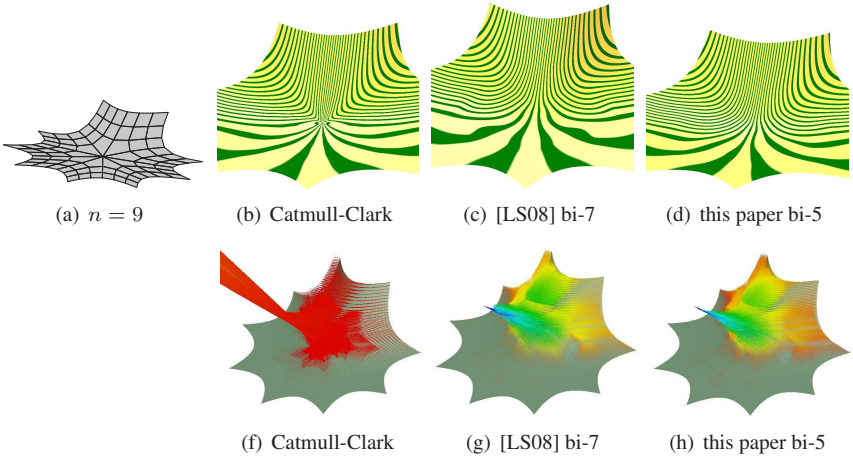

(a) $n = 9$ (b) Catmull-Clark (c) [LS08] bi-7 (d) this paper bi-5

(f) Catmull-Clark (g) [LS08] bi-7 (h) this paper bi-5

Figure 1: **Shape distribution** for three methods, Catmull-Clark subdivision [CC78], the degree bi-7 construction [LS08] and the new degree bi-5 method presented in this paper. The last two methods can fill an n-sided hole in a bi-cubic C^2 tensor-product spline patch complex using n polynomial pieces. Top row: highlight line shading. Bottom row: Gauss-curvature-scaled surface normals. (The Gauss curvature of Catmull-Clark surfaces diverges near the extraordinary point.)

2. Shape and curvature of selected surface constructions

The entertainment industry, led by Pixar, has adopted Catmull-Clark subdivision [CC78] as a main modeling tool. Subdivision is conceptually simple in that it evokes mesh refinement and provides sufficient quality for animation. However, subdivision

surfaces have not entered main stream CAD processing both because they only generalize uniform polynomial splines and because the resulting surfaces consist of infinitely many pieces. The quality of Catmull-Clark subdivision surfaces near the limit point is often poor (Fig. 1e) and the dominant limit shape is always a saddle [KPR04]. [Lev06, KP07] improve the curvature distribution but still use infinitely many surface pieces. A number of surface constructions offer formally high smoothness, but at the cost of a non-standard representation. Examples are global manifold constructions [WP97, GHQ06] and constructions using exponentials [YZ04]. Early spline constructions of G^2 surfaces [Pra97, Rei98, Ye97] were not developed with focus on shape and they are of higher degree: the degree of [Pra97, Rei98] is bi-6 if the surface shape is restricted to be quadratic in a neighborhood of irregular points and bi-9 or higher otherwise. [Ye97] yields degree bi-9. The two low-degree G^2 constructions [GZ99, Pet02a] can suffer from visible shape defects where $n > 5$ patches meet.

To improve shape, functionals of the type

$$\mathcal{F}_\kappa f := \int_0^1 \int_0^1 \sum_{i+j=\kappa, i,j\geq 0} \frac{\kappa!}{i!j!} (\partial_s^i \partial_t^j f(s,t))^2 ds dt. \tag{1}$$

that act on each coordinate of a surface independently, have been advocated as 'fairness' functionals [HKD93, Gre94, Gre96, LGS99, Sar00, WN01]. If the first fundamental form of the resulting surfaces is close to the identity, e.g. if the parameterization is uniform, these functionals can be viewed as penalizing deviation from a surface of low polynomial degree and this may prevent oscillation of the surface and surface normal. Indeed, [LS08] uses an analogue of $\mathcal{F}_4$ to set extraneous degrees of freedom when capping a bi-3 spline complex. The resulting caps of degree bi-7 are generally of high quality but the transition across the boundary of the cap is not as good as it could be, see Fig. 1c, and the case of three patches meeting does not yield satisfactory highlight lines.

3. Definitions and Setup

We consider a network of quadrilateral facets or *quads* to outline the final surface. This is a standard abstraction from the real-life complexity of blending trimmed surfaces. Interior vertices where more or fewer than the regular number of four quads meet are called *irregular nodes*. We assume that each irregular node is surrounded by at least one layer of regular nodes and apply one step of Catmull-Clark subdivision should this not be the case. A *CC-net* $\mathbf{c}$ is a submesh consisting of one irregular node and $6n$ nodes that form two layers of quads surrounding it. (The second layer is allowed to have irregular nodes.) Fig. 2a displays a CC-net and Fig. 2c displays an *extended CC-net* , i.e. CC-net plus one additional layer of quads. This additional layer is not used for the construction of the cap but provides a surface ring (green in Fig. 2d) surrounding the cap for the visual context to judge the transition from the spline complex into the cap. This transition is as important as the quality of the cap itself.

A tensor-product patch $\mathbf{f}$ of bi-degree d is defined by its Bernstein-Bézier (BB)

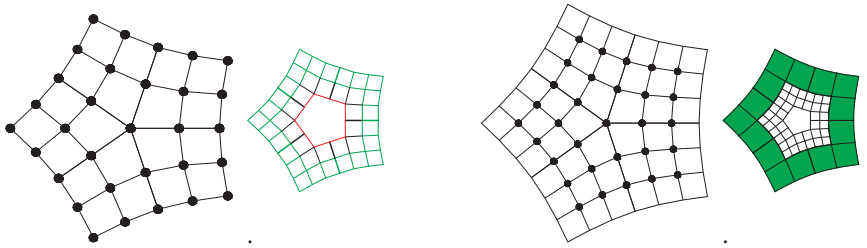

(a) CC-net $\mathbf{c}$ (b) $\mathbf{b}$ (c) extended CC-net (d) bi-3 ring + $\mathbf{b}$

Figure 2: **Input.** (a) A CC-net $\mathbf{c}$ for $n = 5$ or, alternatively, (b) its corresponding **tensor-border** $\mathbf{b}$ of depth 2 represented in terms of BB-coefficients of degree bi-3. (c) Extended CC-net and (d) regular bi-3 surface layer (green) surrounding the tensor-border.

coefficients $\mathbf{f}_{ij}$ as

$$\mathbf{f}(u,v) := \sum_{i=0}^{d}\sum_{j=0}^{d} \mathbf{f}_{ij} B_i^d(u) B_j^d(v)\ , \quad (u,v) \in \square := [0..1]^2, \tag{2}$$

where $B_k^d(t)$ is the kth Bernstein-Bézier polynomial of degree d. Since each 4×4 subgrid of points of the network is interpreted as the B-spline control net of one bicubic piece of a tensor-product spline surface, the well-known formulas of a B-spline to Bernstein-Bézier (BB)-form conversion [Far02, PBP02] can be applied to the CC-net , except at the central irregular point. Along the boundary of the cap, this provides Hermite data in bi-degree 3 form (see Fig. 2b,d). We refer to these Hermite data in the following as the *tensor-border* $\mathbf{b}$ (of depth 2 and degree 3). While our cap will only match the first derivatives defined by $\mathbf{b}$ (after a change of variables), its second-order Hermite data (red layer in Fig. 2b) will serve to propagate curvature from the boundary into the cap.

While the smoothness of the resulting surface can be expressed in the language of differential geometry, i.e. in terms of charts, it suffices, and is often more efficient in the context of modeling, to express smoothness as matching of jets along the boundary where two surface pieces $\mathbf{f}$ and $\tilde{\mathbf{f}}$ are glued together without overlap. G^k continuity of surfaces is established by relating the abutting surface pieces via a reparameterization ρ so that the jets $\partial^k \tilde{\mathbf{f}}$ and $\partial^k(\mathbf{f} \circ \rho)$ of degree k agree. Although ρ represents just a change of variables, its choice crucially influences the properties of the constructed surface cap.

Definition 1. *Two surface pieces* $\tilde{\mathbf{f}}$ *and* $\mathbf{f}$ *sharing a boundary curve* $\mathbf{e}$ *join* G^k *if there is a suitably oriented and non-singular reparameterization* $\rho : \mathbb{R}^2 \to \mathbb{R}^2$ *so that the jets* $\partial^k \tilde{\mathbf{f}}$ *and* $\partial^k(\mathbf{f} \circ \rho)$ *agree along* $\mathbf{e}$*.*

Throughout, we will choose $\mathbf{e}$ to correspond to patch parameters $(u, 0 = v)$. Then the relevant Taylor expansion up to and including degree 1 of the reparameterization ρ with respect to v is

$$\rho := (u + b(u)v, a(u)v). \tag{3}$$

By the chain rule of differentiation, this yields the well-known G^1 constraints (see e.g. [Pet02b])

$$\partial_v \tilde{\mathbf{f}} - a(u)\partial_v \mathbf{f} - b(u)\partial_u \mathbf{f} = 0\,. \tag{4}$$

4. Construction when $n > 4$

In this section we assume that the valence of the irregular point is $n > 4$ and the cap consists of n polynomial pieces of degree bi-5, one per sector. The case $n = 3$ will receive special attention in Section 6. In designing an efficient algorithm, we derive a data-independent component, the reparameterization, based on the valence n.

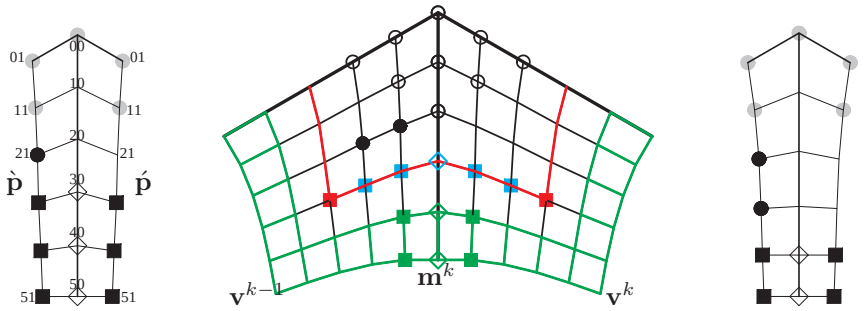

(a) our G^1 (b) two sectors (c) C^1

Figure 3: **Bi-5 cap construction.** (a) Labels along the G^1 strip relevant for the G^1 join between two adjacent patches; black and gray disks, black squares mark BB-coefficients unconstrained after resolving the G^1 constraints (6). (b) Adjacent bi-5 patches of the cap; green = prolongated reparameterized first-order data from $\mathbf{b}$. (c) The standard C^1 transition from the tensor-border offers fewer degrees of freedom.

4.1. Reparameterizing between sectors

Symmetry of construction forces $a(u) := -1$. Our (important) choice for $b(u)$ is

$$b^1(u) := 2\mathsf{c}(1-u)\,,\ \text{where}\ \mathsf{c} := \cos\frac{2\pi}{n}. \tag{5}$$

Then (4) becomes

$$\partial_v \tilde{\mathbf{f}} + \partial_v \mathbf{f} - 2\mathsf{c}(1-u)\partial_u \mathbf{f} = 0\,. \tag{6}$$

We consider two adjacent patches $\grave{\mathbf{p}} := \mathbf{p}^{k-1}$ and $\acute{\mathbf{p}} := \mathbf{p}^k$, $k \in \{0,\ldots,n-1\}$ (superscript modulo n) that join along their shared sector boundary curve $\mathbf{e} = \grave{\mathbf{p}}(u,0) = \acute{\mathbf{p}}(u,0)$ (cf. Fig. 3a). Here it is convenient to index the coefficients of adjacent patches locally and symmetric with respect to $\mathbf{e}$ rather than rotationally symmetric with respect to the irregular point as is appropriate for the full cap in terms of $\mathbf{p}^k$.

Then (6) is enforced between $\grave{\mathbf{p}}$ and $\acute{\mathbf{p}}$ by setting the BB-coefficients (represented as unmarked points or hollow diamonds in Fig. 3a) to

$$\grave{\mathbf{p}}_{10} := \Big(1 - \frac{1}{\mathsf{c}}\Big)\grave{\mathbf{p}}_{00} + \frac{\grave{\mathbf{p}}_{01} + \acute{\mathbf{p}}_{01}}{2\mathsf{c}} \tag{7}$$

$$\grave{\mathbf{p}}_{20} := \Big(1 - \frac{5}{4\mathsf{c}}\Big)\grave{\mathbf{p}}_{10} + \frac{5(\grave{\mathbf{p}}_{11} + \acute{\mathbf{p}}_{11})}{8\mathsf{c}} \tag{8}$$

$$\acute{\mathbf{p}}_{21} := \Big(2 - \frac{6\mathsf{c}}{5}\Big)\grave{\mathbf{p}}_{20} + \frac{6\mathsf{c}}{5}\grave{\mathbf{p}}_{30} - \grave{\mathbf{p}}_{21} \tag{9}$$

$$\grave{\mathbf{p}}_{30} := \frac{5(\grave{\mathbf{p}}_{31} + \acute{\mathbf{p}}_{31}) - 4\mathsf{c}\grave{\mathbf{p}}_{40}}{10 - 4\mathsf{c}} \tag{10}$$

$$\grave{\mathbf{p}}_{40} := \frac{5(\grave{\mathbf{p}}_{41} + \acute{\mathbf{p}}_{41}) - 2\mathsf{c}\grave{\mathbf{p}}_{50}}{10 - 2\mathsf{c}} \tag{11}$$

$$\grave{\mathbf{p}}_{50} := \frac{\grave{\mathbf{p}}_{51} + \acute{\mathbf{p}}_{51}}{2}. \tag{12}$$

All the other BB-coefficients (marked as black or gray disks or black squares in Fig. 3a) remain unconstrained in this *local* solution – the interaction around the irregular point is described in Section 4.3.

4.2. Reparameterizing the tensor-border $\mathbf{b}$

Equation (12) reflects the fact that the pieces of $\mathbf{b}$ are smoothly connected spline pieces. By contrast, (11) does not equate derivatives but requires a reparameterization β of the tensor-boundary data $\mathbf{b}$ of depth 1 (green layers in Fig. 2b) in order to verify that the cap joins G^1 with the surrounding bi-3 splines. This reparameterization β is important for the quality of final surface.

We label the BB-coefficient corresponding to the corner $\mathbf{v}^{k-1}$ of the n-sided hole as β_{00} (see Fig. 4) and the one corresponding to the neighboring (mid-edge) $\mathbf{m}^k$ as β_{30} in Fig. 4b, respectively β_{40} in Fig. 4c. We choose β to have sufficiently many degrees of freedom for its role in (4), to respect the symmetry of the regular tensor-product layout of the tensor-border $\mathbf{b}$ at $\mathbf{v}^{k-1}$ and construct β symmetric with respect to the diagonal $u = v$. The resulting terms in the G^1 constraints (4) are

$$a(u) := \sum_{i=0}^{2} a_i B_i^2(u), \quad b(u) := \sum_{i=0}^{3} b_i B_i^3(u), \tag{13}$$

$$a_0 := 1,\ a_1 := (1 - \frac{\mathsf{c}}{2})a_2;\ b_0 := 0,\ b_1 := \frac{(2-\mathsf{c})a_2 - 2}{3},\ b_3 := 0.$$

Then $\mathbf{b} \circ \beta$ is of degree 5 and for any choice of a_2 and b_2 we have pinned down the BB-coefficients (marked as green squares or hollow diamonds in Fig. 3b) so they satisfy (11) and (12). Our default choices are

$$b_2^{def} := 0, \quad a_2^{def} := 1 + 0.413\mathsf{c} + 0.116\mathsf{c}^2, \quad \text{where } \mathsf{c} := \cos\frac{2\pi}{n}. \tag{14}$$

Here $b_2 = 0$ enforces that $\overline{\beta_{20}\beta_{21}}$ is parallel to v-direction of the unit square and a_2^{def} improves the uniformity of the layout of BB-coefficients as explained in the next

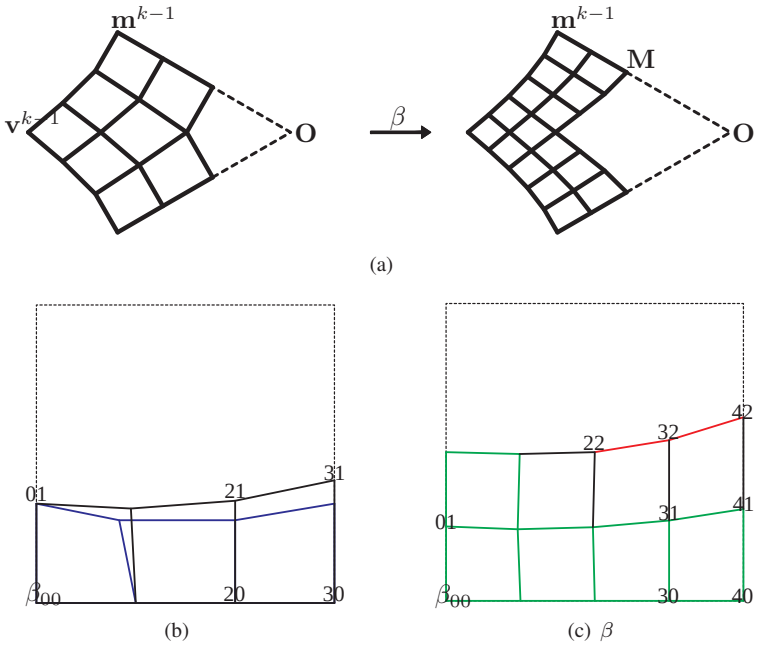

Figure 4: **Reparameterization β of input tensor-border $\mathbf{b}$** here for $n = 6$. (a) The stretch-minimizing reparameterization of the tensor-border of χ_{CC} motivates the choice of a_2^{def}. (b) BB-coefficients and control net of β up to first order. Black = using a_2^{def}, blue = using $a_2 = 1$. (c) β up to second order (the first order expansion is degree-raised to degree 4).

section. When the tensor-border data are taken from

χ_{CC}, the Catmull-Clark subdivision characteristic map (see e.g. [PR08]),

the result is the layout of BB-coefficients β_{ij}, $i = 0, \ldots, 3$, $j = 0, 1$ shown in Fig. 4a,*right*. Fig. 4b shows β with a_2^{def} as a black net; the overlaid blue net corresponds to choosing $a_2 = 1$. The choice $a_2 = 1$ used in [LS08] leads to the quality problems observed in Fig. 1b.

Since we want to prolong the curvature information of the tensor-border into the cap, we define β up to second order. We express the first-order layers in degree 4 form (by degree-raising, see the green layers in Fig. 4c). Respecting the symmetry of the regular tensor-product layout of the tensor-border and (10), we set

$$\beta_{22} := \left(\frac{1}{2}, \frac{1}{2}\right), \quad \beta_{i2} := 2\beta_{i1} - \beta_{i0},\ i = 3, 4. \tag{15}$$

Since the degree in u of the second-order expansion with respect to v of $\mathbf{g} := \mathbf{b} \circ \beta$ exceeds 5, we collect from $\mathbf{g}$ only the tensor 2-jets

$$\left[\frac{d^{ij}\mathbf{g}}{(du)^i (dv)^j}\right]_{i,j \in \{0,1,2\}} \tag{16}$$

expressed as 3×3 coefficients in bi-5 BB-form at $\mathbf{v}^{k-1}$ and $\mathbf{m}^k$. These coefficients satisfy (10) for any choice of a_2 and define a second-order extension of the boundary data. To space the BB control points uniformly, we set a_2 as in (14) so that $M \approx (2\mathbf{O} + 3\mathbf{m}^k)/5$ (see Fig. 4a).

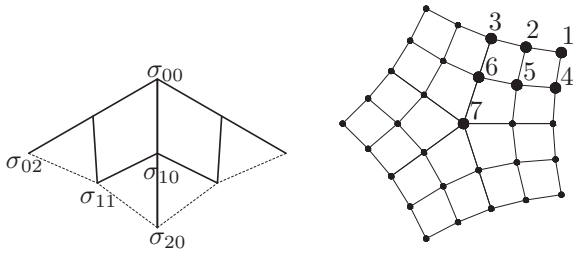

(a) $J_2\sigma$ (b) CC-net indices

Figure 5: (a) Reparameterization σ near the origin. (b) the irregular point has the label $\mathbf{c}_7^k$.

4.3. Curvature continuity at the irregular point

While enforcing G^1 constraints leaves free the BB-coefficients $\mathbf{p}_{11}^k$, this extra freedom is difficult to harness and various heuristics almost invariably result in shape artifacts in the vicinity of the irregular point, such as bunched up or oscillating highlight lines. These artifacts intensify with increasing n. A remedy is to enforce curvature continuity at the irregular point. Let $\sigma : [0..1]^2 \to \mathbb{R}^2$ be a bi-5 map with BB-coefficients σ_{ij} and $J_2\sigma := [\sigma_{ij}]_{i+j\leq 2}$ where $\sigma_{00} = (0, 0)$ (see Fig. 5a) define the second-order jet at the origin. Then $J_2\sigma$ is determined by (7), (8), symmetry and by enforcing uniform spacing $\sigma_{20} := 2\sigma_{10}$ so that $\sigma_{11} := \frac{5+4\mathsf{c}}{5(1+\mathsf{c})}\frac{\sigma_{20}+\sigma_{02}}{2}$. Copies of $J_2\sigma$ rotated by $\frac{2\pi k}{n}$ form the jets of the bi-5 maps σ^k, $k = 0, .., n-1$ that surround the origin. For a quadratic map $\mathbf{q}$ (whose six coefficients will be determined as part of a final functional minimization (17)), the partial derivatives $[\frac{d^{ij}(\mathbf{q}\circ\sigma^k)}{(du)^i(dv)^j}]_{i+j\leq 2}$ at the origin are expressed in bi-5 BB-form as $[\mathbf{p}_{ij}^k]_{i+j\leq 2}$. By this construction, the patches $\mathbf{p}^k$ join with matching curvature at the irregular point and it is easy to check that the $\mathbf{p}_{ij}^k$, $i + j \leq 2$, $k = 0, \ldots, n-1$, satisfy (7) and (8).

4.4. The complete Algorithm when $n > 4$

Here we summarize the steps explained in the previous subsections.

Input: A CC-net of $6n + 1$ points $\mathbf{c}_j^k$, $j = 1, \ldots, 7$, $k = 0, \ldots, n-1$, with irregular node $\mathbf{c}_7^0$ of valence n (cf. Fig. 5b) – **or** – a tensor-border $\mathbf{b}$ of degree 3 and depth 2 (cf. Fig. 2b).

Output: A surface cap $\mathbf{p}$ consisting of n bi-5 patches $\mathbf{p}^k$, $k = 0, \ldots, n-1$. The patches $\mathbf{p}^{k-1}$ and $\mathbf{p}^k$ are joined G^1 and join G^1 with $\mathbf{b}$.

Algorithm

1. Set the irregular point to the limit point of Catmull-Clark subdivision [HDK93]

$$\mathbf{q}_{00} := \frac{n}{n+5}\mathbf{c}_7^0 + \sum_{i=0}^{n-1}(\gamma_5\mathbf{c}_5^i + \gamma_6\mathbf{c}_6^i), \quad \gamma_5 := \frac{1}{n(n+5)},\ \gamma_6 := \frac{4}{n(n+5)}.$$

2. Set the depth 2 tensor-border of $\mathbf{p}$ to that of $\mathbf{b} \circ \beta$.

3. Let $\mathcal{P} := \{\mathbf{q}_{ij}, \mathbf{p}_{12}^k, \mathbf{p}_{22}^k\}$, $k = 0, \ldots, n-1$, $0 < i + j \leq 2$ (see black disks in Fig. 3b). Express $\acute{\mathbf{p}}_{21}$ according to (9) and $\mathbf{p}_{ij}^k$, $i + j \leq 2$ (circled coefficients in Fig. 3b) in terms of the coefficients in $\mathcal{P}$ and determine $\mathcal{P}$ by minimizing the functional (1) with respect to $\mathcal{P}$:

$$\min_{\mathcal{P}} \sum_{k=0}^{n-1} \mathcal{F}_4(\mathbf{p}^k). \tag{17}$$

4.5. Implementation via generating functions

Due to the relatively short, explicit formulas for the dependent BB-coefficients in terms of the independent BB-coefficients, the construction steps are simple and stable. With the irregular point set to the Catmull-Clark limit point of the CC-net , (17) requires only solving a linear system of size $N \times N$, where $N := 2n + 5$. For $5 \leq n \leq 12$, we computed and tabulated the seven *generating functions of the CC-net* . The final surface cap is a linear combination of these tabulated generating functions, weighted by their CC-net points.

Specifically, since the Algorithm works for each coordinate separately, it can be applied when all CC-net points $\mathbf{c}_m$ have value 0, except for $\mathbf{c}_m^0 = 1$, for one of $m = 1, \ldots, 7$ (see Fig. 5b). This yields the scalar-valued bi-5 coefficients

$$h_{ij}^{\ell,m} \in \mathbb{R}, \quad \ell = 0, \ldots, n-1,\ m = 1, \ldots, 7,\ i, j \in \{0, \ldots, 5\}, \tag{18}$$

where $h_{ij}^{0,7} = \ldots = h_{ij}^{n-1,7}$. Then the BB-coefficients are

$$\mathbf{p}_{ij}^{\kappa} := h_{ij}^{0,7}\mathbf{c}_7^0 + \sum_{\ell=0}^{n-1}\sum_{m=1}^{6} h_{ij}^{\ell,m}\mathbf{c}_m^{\kappa-\ell}, \tag{19}$$

where the superscript of $\mathbf{c}_m^{\kappa-\ell}$ is interpreted modulo n. Since more than half of each patch is determined by the simple formulas of $\mathbf{b} \circ \beta$ only the remaining coefficients need to be tabulated.

5. Discussion of the algorithmic decisions

Our choice $b^1(u) := 2\mathsf{c}(1-u)$ for G^1 continuity between sectors in Section 4.1 distinguishes the construction from almost all piecewise polynomial constructions in the literature. The exceptions, [Pet93] and [Rei95], were not derived with an emphasis on good shape but to minimize polynomial degree. (The recent publication [KP14] was inspired by the present, earlier construction, but was developed and optimized for

bi-2 splines and inner surfaces with lower expectations of smoothness. A comparison is presented later in this section.)

The standard approach found in the remaining literature extrapolates the tensor-border without reparameterization and hence chooses $b^2(u) := 2\mathsf{c}(1-u)^2$. This choice leaves fewer free coefficients (compare Fig. 3a to Fig. 3c) and looses essential degrees of freedom for constructing a high-quality cap of degree bi-5: the arrows in Fig. 6b point out unwanted kinks in the highlight lines at the tensor-border transitions when b^2 is used and Fig. 6e shows abrupt curvature transitions.

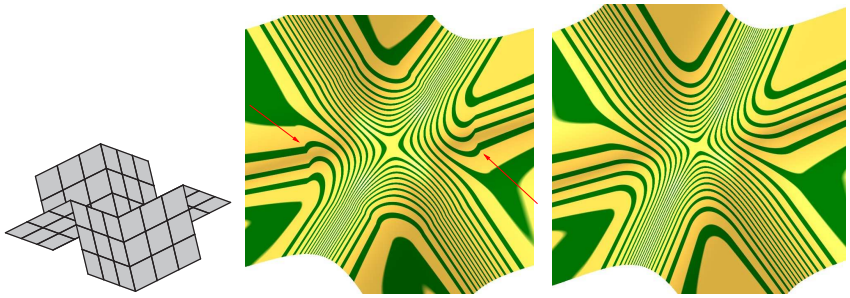

(a) CC-net (b) b^2 (c) b^1

(e) b^2 (f) b^1

Figure 6: **Border reparameterization.** Our cap using $b^1(u) := 2\mathsf{c}(1-u)$ vs the standard construction using $b^2(u) := 2\mathsf{c}(1-u)^2$. (b,c) highlight shading; (d,e) mean curvature. Note the oscillation of highlight lines (marked by red arrows) and the less graceful transition of curvature for b^2.

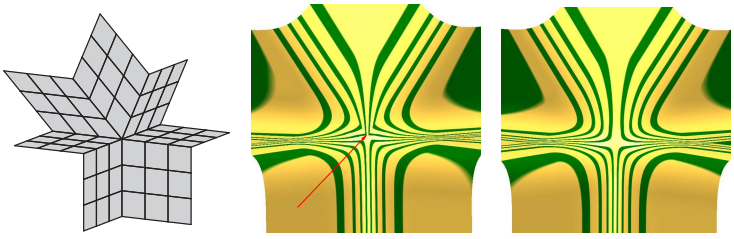

(a) $n = 7$ CC-net (b) G^1-eop (c) G^2-eop

Figure 7: **Curvature continuity at the irregular point** (G^2-eop) vs. tangent continuity (G^1-eop).

While for valencies $n = 5, 6$ the difference between prescribing G^1 continuity at the irregular point and prescribing G^2 as in our construction is not pronounced, starting

with valence $n = 7$ the advantage of curvature continuity at the center is clearly visible: note the sharp turns of the highlight lines in Fig. 7b vs. Fig. 7c.

To bring out any weakness of the constructions, we use extreme input CC-nets [KP15]. One example of valence $n = 6$ is Fig. 8a. Parts of the CC-net are intentionally planar to assure easily-understood, namely zero curvature (If the tensor-border has itself a complex curvature distribution, it will be more difficult to predict the expected or desirable curvature distribution of the surface cap.) The comparison between Fig. 8c and Fig. 8d re-confirms the advantage of reparameterizing linearly with b^1 rather than quadratically with b^2. Fig. 8b,d illustrates the advantage of prolonging the curvature from the tensor-border $\mathbf{b}$ into the cap. We soften the CC-net of Fig. 8a to Fig. 8e by applying two Catmull-Clark refinement steps. Even for this more gentle input, we can observe the artifacts. The highlight lines of Catmull-Clark subdivision strongly oscillate near the irregular point.

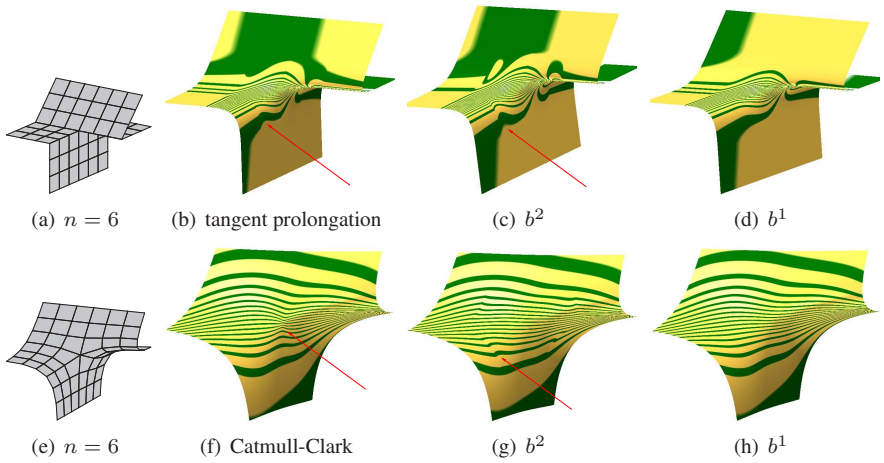

(a) $n = 6$ (b) tangent prolongation (c) b^2 (d) b^1

(e) $n = 6$ (f) Catmull-Clark (g) b^2 (h) b^1

Figure 8: **Prolongation of shape from the tensor-border.** (b) prolonging only the tangent information of the tensor-border $\mathbf{b}$ leads to sharp highlight line transitions from the tensor-border. (c) Prolonging curvature information using $b^2(u) := 2\mathsf{c}(1-u)^2$; (d) prolonging curvature information using $b^1 := 2\mathsf{c}(1-u)$ (our construction); (f) Catmull-Clark: note the pinched highlight lines near the irregular point. (g) b^2: note the kinks in the highlight lines at the cap boundary.

To choose our functional in (17), we compared highlight lines when the constructions were applied to the obstacle course of input meshes [KP15]. For example, the arrow in Fig. 9b points to undesirable abrupt changes in the highlight lines when the second best choice, $\mathcal{F}_3$, is used in place of our choice $\mathcal{F}_4$.

Another class of challenging CC-nets in the obstacle course consist of a simple base shape, here a plane, perturbed by pulling out one mesh point as in Fig. 10a,b. This yields the surfaces Fig. 10d and Fig. 10e. In Fig. 10e, for $n = 8$, oscillations start forming in the transition between the bi-3 splines and the bi-5 cap. We do not work to improve shape here since the artifact disappears after applying one Catmull-Clark subdivision step (see Fig. 10c yielding Fig. 10f). The CC-net of Fig. 11a is that of Fig. 1a. It is the result of applying two steps of Catmull-Clark refinement to an extreme configuration where seven sectors lie in one plane and two sectors rise up.

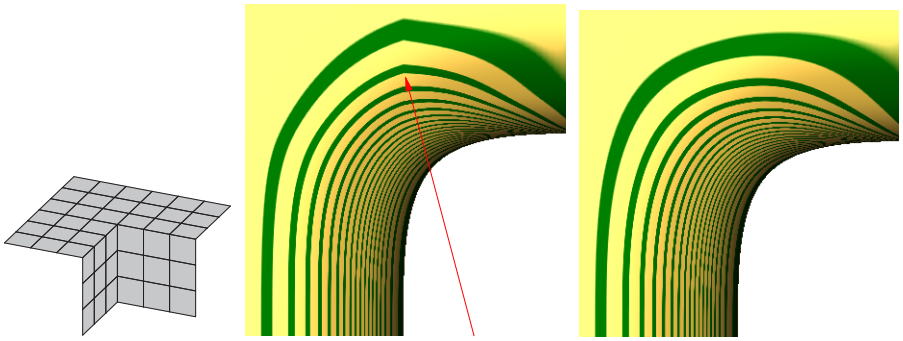

(a) CC-net $n = 5$ (b) $\mathcal{F}_3$ (c) our $\mathcal{F}_4$

Figure 9: Two-beam corner blend for different **functionals.** Note the kink in the highlight line along the center of (b).

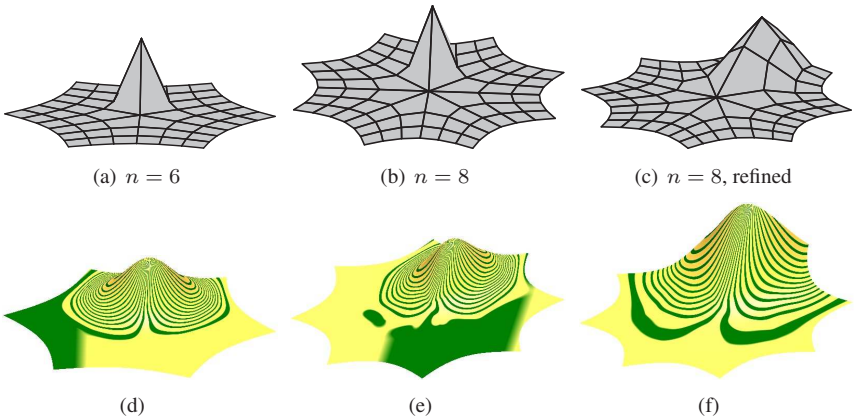

(a) $n = 6$ (b) $n = 8$ (c) $n = 8$, refined

(d) (e) (f)

Figure 10: The planar base mesh of χ_{CC} perturbed by moving one mesh point. The CC-net (c) is obtained from (b) by one Catmull-Clark refinement step. (d,e,f) Highlight line shading.

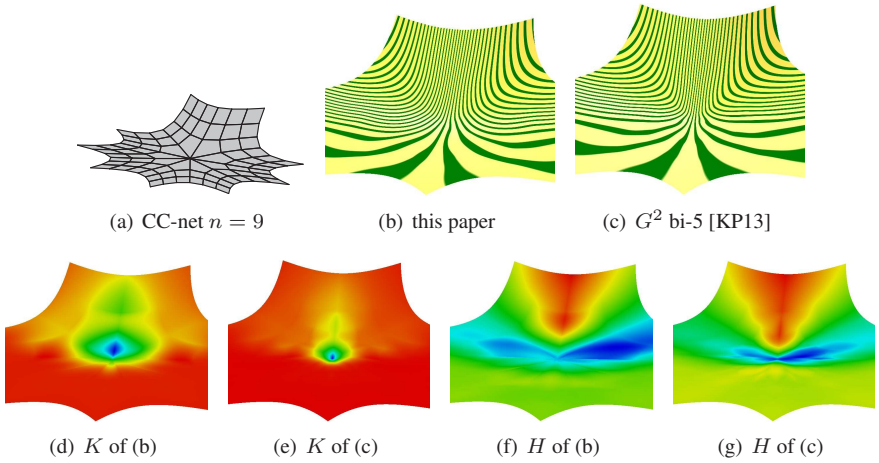

(a) CC-net $n = 9$ (b) this paper (c) G^2 bi-5 [KP13]

(d) K of (b) (e) K of (c) (f) H of (b) (g) H of (c)

Figure 11: Comparison with a curvature continuous cap construction [KP13] of the same degree but seven times as many pieces. K = Gauss curvature, H = Mean curvature shading. Fig. 1 uses the same input.

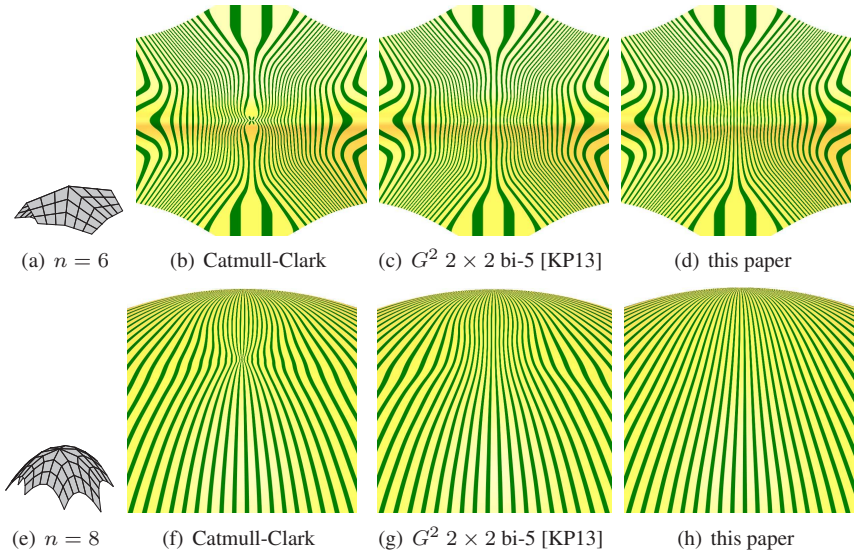

(a) $n = 6$ (b) Catmull-Clark (c) G^2 2×2 bi-5 [KP13] (d) this paper

(e) $n = 8$ (f) Catmull-Clark (g) G^2 2×2 bi-5 [KP13] (h) this paper

Figure 12: Convex input CC-nets.

Here we focus on comparing our G^1 bi-5 cap construction consisting of n patches to the G^2 bi-5 cap from [KP13] that uses a ternary split resulting in $7n$ patches for valence $n = 9$. The curvature distributions of G^1 bi-5 surface is competitive with its considerably more complex G^2 bi-5 counterpart.

In Fig. 12, we input a convex CC-net approximating a paraboloid. Catmull-Clark subdivision is known to not preserve convexity and shading reveals pinched and oscillating highlight lines. The highlight line distribution of our G^1 bi-5 construction is on par with the G^2 bi-5 construction [KP13]. We conclude by comparing to a simi-

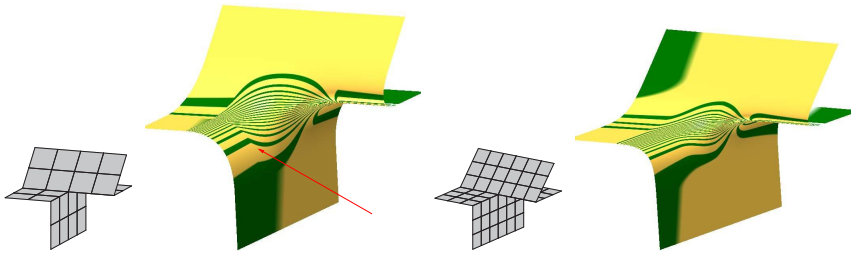

(a) $n = 6$ (b) [KP14] bi-4 (c) $n = 6$ (d) this paper, bi-5

Figure 13: The input net (a) for [KP14] is a sub-net of our CC-net (c).

lar construction generalizing bi-2 C^1 splines [KP14]. Given the lower smoothness of the underlying spline and cap, [KP14] unsurprisingly yields sharper transitions that are incompatible with class A surfaces (see arrow in Fig. 13b).

6. Valence $n = 3$: bi-4 capping

Valence $n = 3$ typically requires special consideration but often offers the opportunity of constructing caps of lower-degree. We found that a cap of degree bi-4 performs remarkably well. We repeat the steps of the main construction adjusted to the bi-4 cap.

6.1. G^1 join between sectors

With the notation of Section 4.1 (cf. Fig. 14a) and $\rho := -(1-u)$ since $\mathsf{c} := -\frac{1}{2}$ for $n = 3$, we enforce (6) between two sectors $\grave{\mathbf{p}}$ and $\acute{\mathbf{p}}$ by setting

$$\grave{\mathbf{p}}_{10} := 3\grave{\mathbf{p}}_{00} - \grave{\mathbf{p}}_{01} - \acute{\mathbf{p}}_{01}; \tag{20}$$

$$\grave{\mathbf{p}}_{40} := \frac{\grave{\mathbf{p}}_{41} + \acute{\mathbf{p}}_{41}}{2}; \tag{21}$$

$$\grave{\mathbf{p}}_{30} := \frac{4}{9}(\grave{\mathbf{p}}_{31} + \acute{\mathbf{p}}_{31}) + \frac{1}{18}(\grave{\mathbf{p}}_{41} + \acute{\mathbf{p}}_{41}); \tag{22}$$

$$\grave{\mathbf{p}}_{20} := \frac{2}{5}(\grave{\mathbf{p}}_{21} + \acute{\mathbf{p}}_{21}) + \frac{4}{45}(\grave{\mathbf{p}}_{31} + \acute{\mathbf{p}}_{31}) + \frac{1}{90}(\grave{\mathbf{p}}_{41} + \acute{\mathbf{p}}_{41}); \tag{23}$$

and are left with the constraint

$$\begin{aligned} 120(\grave{\mathbf{p}}_{11} + \acute{\mathbf{p}}_{11}) - 990\grave{\mathbf{p}}_{00} + 330(\grave{\mathbf{p}}_{01} + \acute{\mathbf{p}}_{01}) \\ + 36(\grave{\mathbf{p}}_{21} + \acute{\mathbf{p}}_{21}) + 8(\grave{\mathbf{p}}_{31} + \acute{\mathbf{p}}_{31}) + \grave{\mathbf{p}}_{41} + \acute{\mathbf{p}}_{41} = 0 \end{aligned} \tag{24}$$

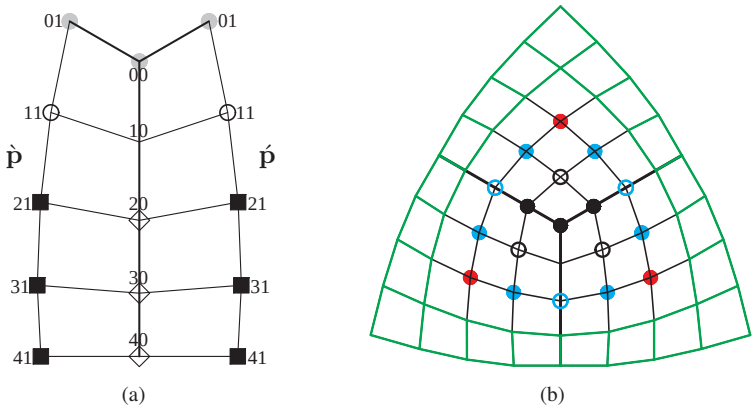

Figure 14: **Bi-4 cap construction.** (a) G^1 strip. (b) BB-coefficients of the bi-4 cap: solid disks are unconstrained by smoothness while the green boundary coefficients are determined by $\mathbf{b} \circ \beta$.

for each of the three sector boundaries. The 3×3 system of linear equations of type (24) with to respect $\mathbf{p}_{11}^k$, $k = 0, 1, 2$ has a unique solution.

6.2. Reparameterizing the tensor-border $\mathbf{b}$

Equation (21) reflects the fact that the pieces of $\mathbf{b}$ are smoothly connected splines. By contrast, (22) requires a reparameterization β of the tensor-boundary data $\mathbf{b}$ of depth 1. Here we can use the unique symmetric reparameterization β of degree 2 with $a(u) := 1 - \frac{1}{3}u$, $b(u) := -\frac{1}{3}(1-u)u$ whose BB-coefficients are shown in Fig. 15a. We degree-raise the depth 1 representation of β to bi-4 (green in Fig. 15b), observe that the points β_{02}, β_{12} are defined by symmetry with respect to the diagonal $u = v$ and that this symmetry also implies $\beta_{22} := (Z, Z)$ for some Z. For any $\beta_{32} := (X, Y)$, setting $\beta_{42} := (1, \frac{4}{5}Y + \frac{1}{30})$ enforces (23).

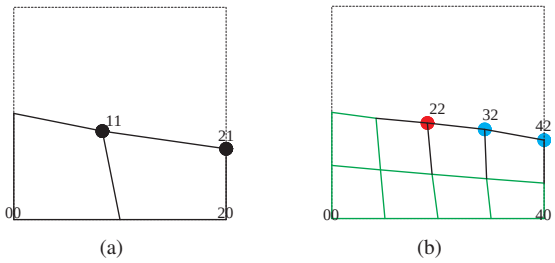

Figure 15: **Reparameterization β of input tensor-border $\mathbf{b}$.** (a) Black – reparameterization for depth 1 part. (b) Extended β for the second order Hermite data.

Since the degree in u of the second order expansion with respect v of $\mathbf{b} \circ \beta$ now exceeds 4, we collect from $\mathbf{b} \circ \beta$ only the tensor 2-jets at $\mathbf{v}^{k-1}$ and $\mathbf{m}^k$ expressed as 3×3 coefficients in bi-4 BB-form (cf. (16)). This defines the BB-coefficients marked

by red or cyan disks or cyan circles in Fig. 14b. The default values of the parameters

$$X^{def} := 0.72\,, \quad Y^{def} := 0.42\,, \quad Z^{def} := 0.45,$$

are chosen to closely approximate the BB-coefficients $\sigma_{22} \in \mathbb{R}^2$ and σ_{32}, where σ is constructed as follows: set the tensor-border of σ to the tensor-border of $\chi_{CC} \circ \beta$, express the coefficients of the G^1 strip between sectors in terms of $\mathcal{P}$ (see Section 6.1) and compute the elements of $\mathcal{P}$ by minimizing $\sum_{k=0}^{2} \mathcal{F}_4(\sigma^k)$. Note that $\mathcal{P}$ includes σ_{22}, σ_{12} and σ_{21} (solid disks in in Fig. 14b).

6.3. The complete Algorithm when $n = 3$

1. Set the irregular point to

$$(1 - 3\gamma_5 - 3\gamma_6)\mathbf{c}_7^0 + \sum_{i=0}^{2}(\gamma_5 \mathbf{c}_5^i + \gamma_6 \mathbf{c}_6^i), \quad \gamma_5 := \frac{5}{96},\ \gamma_6 := \frac{1}{6}. \tag{25}$$

2. Set the depth 2 tensor-border of $\mathbf{p}$ to match $\mathbf{b} \circ \beta$.

3. Let $\mathcal{P} := \{\mathbf{p}_{10}^1, \mathbf{p}_{10}^2\}$. Express $\mathbf{p}_{10}^0$ in terms of $\mathcal{P}$ to satisfy (20) and $\mathbf{p}_{11}^k$ in terms of $\mathcal{P}$ to satisfy (24) and determine the BB-coefficients in $\mathcal{P}$ by minimizing $\sum_{k=0}^{2} \mathcal{F}_4(\mathbf{p}^k)$.

Note that for implementation via generating functions only the two elements of $\mathcal{P}$ need to be tabulated since the remaining are expressed by simple formulas.

6.4. Curvature continuity at the irregular point when $n = 3$

Unlike when $n > 4$, for $n = 3$ there is no need to enforce curvature continuity at the irregular point.

Theorem 1. *For valence $n = 3$ any piecewise polynomial smooth capping, satisfying the symmetric constraints* (4) *with $a(u) := -1$ is curvature continuous at the irregular point.*

Proof We show that the second-order expansions $[\mathbf{p}_{ij}^k]_{i+j\le 2}$ of the $n = 3$ patches joining with tangent continuity at the irregular point define a unique 2-jet $J_2\mathbf{q}$.

With the notations of Section 4 and denoting the bi-degree of the cap $\mathbf{p}$ by m, tangent plane continuity and symmetry at the irregular point imply that (20) holds for a $b(u)$ with first-order expansion $-1 + eu$. Then (4) implies

$$\grave{\mathbf{p}}_{20} := \frac{9m + 2e - 5}{m - 1}\grave{\mathbf{p}}_{00} + \frac{2 - 3m - e}{m - 1}(\grave{\mathbf{p}}_{01} + \acute{\mathbf{p}}_{01}) - \frac{m}{m - 1}(\grave{\mathbf{p}}_{11} + \acute{\mathbf{p}}_{11}). \tag{26}$$

Analogous to Section 4.3, we construct $J_2\sigma$ by determining σ_{ij}, $i + j \le 2$, in BB-form of degree bi-m so that (20) and (26) hold. In particular, $\sigma_{11} := (1 + \frac{e}{m})\frac{\sigma_{02}+\sigma_{20}}{2}$. Then the partial derivatives $[\frac{d^{ij}(\mathbf{q}\circ\sigma^k)}{(du)^i(dv)^j}]_{i+j\le 2}$, at the origin are expressed in BB-form of degree bi-m as $[\bar{\mathbf{p}}_{ij}^k]_{i+j\le 2}$ (with $\mathbf{q}$ in symbolic form). By inspection, the six relevant degrees of freedom of $\mathbf{q}$ can be chosen so that $\bar{\mathbf{p}}_{ij}^k = \mathbf{p}_{ij}^k$. |||

6.5. Comparison

Although formally only G^1, the construction of degree bi-4 compares well with the more complex G^2 constructions of [KP13] (bi-6) and [LS08] (bi-7). Remarkably, for the challenge examples, e.g. Fig. 16, the bi-4 cap exhibits a more uniform curvature variation than its G^2 competitors. The problems of [LS08] can be traced back to setting the irregular point to the Catmull-Clark limit point. The difference to our irregular point, which coincides with that of [KP13], is a small change in the parameter γ_5 of (25):

$$\gamma_5^{CC} := \frac{4}{96} = \frac{1}{24}, \quad \gamma_5^{our} := \frac{5}{96}.$$

Our choice of $5/96$ over $4/96$ was established by binary search, for several inputs, and by opting for the simplest expression: sampling near $5/96$ does not show noticeable differences but sampling further away, say at $4.5/96$ results in worse highlight lines (cf. Fig. 17).

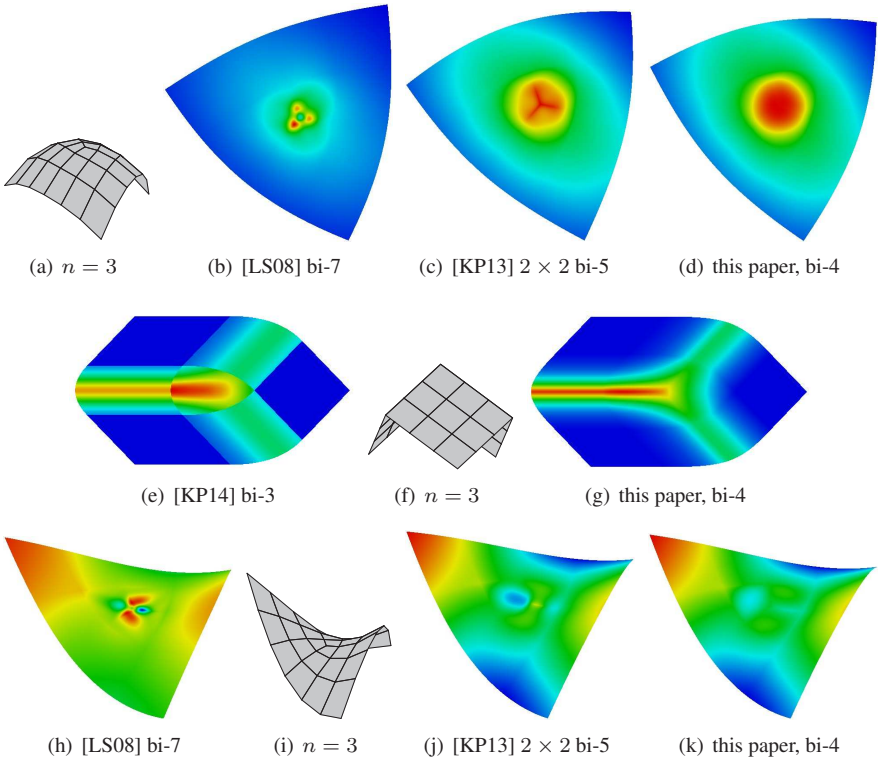

(a) $n = 3$ (b) [LS08] bi-7 (c) [KP13] 2×2 bi-5 (d) this paper, bi-4

(e) [KP14] bi-3 (f) $n = 3$ (g) this paper, bi-4

(h) [LS08] bi-7 (i) $n = 3$ (j) [KP13] 2×2 bi-5 (k) this paper, bi-4

Figure 16: Top row: convex input and Gauss curvature shading. Middle row: convex input and highlight line shading. Bottom row: saddle input and mean curvature shading.

Since convex caps are the dominant scenario when $n = 3$, Fig. 16 compares our construction with such an input. Fig. 16h,i,j, the saddle analogue of Fig. 16b,c,d, yields

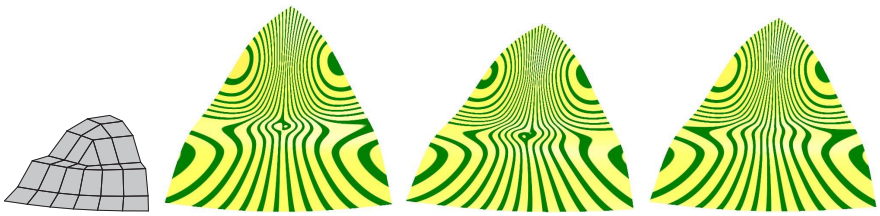

(a) CC-net (b) Catmull-Clark (c) bi-4 with CC-eop (d) our bi-4

Figure 17: The **importance of setting the irregular point when $n = 3$.** While the step (oscillation) in the input CC-net implies a large scale oscillation in the highlight lines, Catmull-Clark surfaces and the bi-4 construction using the Catmull-Clark limit point show an additional oscillation near the irregular point.

the same quality assessment. Fig. 16e,g confirm qualitative difference between our bi-5 cap to the caps of [KP14]. Generalizing C^1 bi-2 splines rather than C^2 bi-3 splines, [KP14] was introduced for inner surfaces, not class A surfaces where highlight lines have to vary smoothly unless explicitly designed otherwise.

Finally, Fig. 17 illustrates the impact γ_5 on the quality of valence 3 surfaces, confirming the advantage of our choice over the Catmull-Clark choice.

7. Conclusions

Although the presented surface construction only guarantees tangent continuity, it carefully leverages the interplay of parameterization and shape to generate caps whose visual, highlight line and even curvature quality is comparable and, at times, superior to more complex curvature continuous constructions. Key construction principles are increased smoothness at the irregular point and immediate reparameterization of all boundary data to better extend shape into the multi-sided cap.

The n-sided caps constructed by the algorithm in this paper are of degree bi-5 in the general case and of only degree bi-4 when $n = 3$. They consist of only n pieces. The low degree and high flexibility make the new construction easy to use for iso-geometric analysis as demonstrated in [NKP14].

Acknowledgments.

The work was supported in part by NSF Grant CCF-1117695. Charles Loop kindly provided the generating functions for the comparisons with [LS08].

[CC78] E. Catmull and J. Clark. Recursively generated B-spline surfaces on arbitrary topological meshes. *Computer-Aided Design*, 10:350–355, September 1978.

[Far02] G. Farin. *Curves and Surfaces for Computer Aided Geometric Design: A Practical Guide*. Academic Press, San Diego, 2002.

[GHQ06] Xianfeng Gu, Ying He, and Hong Qin. Manifold splines. *Graphical Models*, 68(3):237–254, 2006.

[Gre94] G. Greiner. Variational design and fairing of spline surfaces. *Computer Graphics Forum*, 13(3):143–154, 1994.

[Gre96] G. Greiner. Curvature approximation with application to surface modeling. In J. Hoschek and P. Kaklis, editors, *Advanced Course on FAIRSHAPE*. B. G. Teubner, 1996.

[GZ99] John A. Gregory and Jianwei Zhou. Irregular C^2 surface construction using bi-polynomial rectangular patches. *Comp Aided Geom Design*, 16(5):423–435, 1999.

[HKD93] Mark Halstead, Michael Kass, and Tony DeRose. Efficient, fair interpolation using Catmull-Clark surfaces. In *Proc 20th Annual Conference on Computer Graphics and Interactive Techniques*, SIGGRAPH '93, pages 35–44, New York, NY, USA, 1993. ACM.

[KP07] K. Karčiauskas and J. Peters. Concentric tesselation maps and curvature continuous guided surfaces. *Computer Aided Geometric Design*, 24(2):99–111, Feb 2007.

[KP09] K. Karčiauskas and J. Peters. Guided spline surfaces. *Comp Aided Geom Design*, 26(1):105 – 116, 2009.

[KP13] K. Karčiauskas and J. Peters. Biquintic G^2 surfaces. In G. Mullineux Robert J. Cripps and M. A. Sabin, editors, *The Mathematics of Surfaces XIV*, pages 213–236. The Institute of Mathematics and its Applications, September 2013.

[KP14] Kęstutis Karčiauskas and Jörg Peters. Smooth multi-sided blending of biquadratic splines. *Computers and Graphics*, SMI 2014 Hongkong, 2014.

[KP15] Kęstutis Karčiauskas and Jörg Peters. Quad cc-net obstacle course, 2015. http://www.cise.ufl.edu/research/SurfLab/shape_gallery.shtml.

[KPR04] K. Karciauskas, J. Peters, and U. Reif. Shape characterization of subdivision surfaces – case studies. *Computer Aided Geometric Design*, 21(6):601–614, july 2004.

[Lev06] Adi Levin. Modified subdivision surfaces with continuous curvature. *ACM Trans. Graph*, 25(3):1035–1040, 2006.

[LGS99] J. Loos, G. Greiner, and H-P. Seidel. Modeling of surfaces with fair reflection line pattern. In Bob Werner, editor, *Proceedings of the International Conference on Shape Modeling and Applications (SMI-99)*, pages 256–263, Los Alamitos, CA, March 1–4 1999. IEEE Computer Society.

[LS08] Charles T. Loop and Scott Schaefer. G^2 tensor product splines over extraordinary vertices. *Comput. Graph. Forum*, 27(5):1373–1382, 2008.

[NKP14] Thien Nguyen, Kęstutis Karčiauskas, and Jörg Peters. A comparative study of several classical, discrete differential and isogeometric methods for solving poisson's equation on the disk. *Axioms*, 3(2):280–299, 2014.

[PBP02] Hartmut Prautzsch, Wolfgang Boehm, and Marco Paluszny. *Bézier and B-spline techniques*. Springer Verlag, 2002.

[Pet93] J. Peters. Smooth free-form surfaces over irregular meshes generalizing quadratic splines. *Computer Aided Geometric Design*, 10:347–361, 1993.

[Pet02a] J. Peters. C^2 free-form surfaces of degree (3,5). *Comp Aided Geom Design*, 19(2):113–126, 2002.

[Pet02b] J. Peters. Geometric continuity. In *Handbook of Computer Aided Geometric Design*, pages 193–229. Elsevier, 2002.

[PR08] J. Peters and U. Reif. *Subdivision Surfaces*, volume 3 of *Geometry and Computing*. Springer-Verlag, New York, 2008.

[Pra97] H. Prautzsch. Freeform splines. *Comput. Aided Geom. Design*, 14(3):201–206, 1997.

[Rei95] Ulrich Reif. Biquadratic G-spline surfaces. *Computer Aided Geometric Design*, 12(2):193–205, 1995.

[Rei98] U. Reif. TURBS—topologically unrestricted rational B-splines. *Constr. Approx.*, 14(1):57–77, 1998.

[Sar00] Ramon F. Sarraga. A variational method to model G^1 surfaces over triangular meshes of arbitrary topology in R^3. *ACM Trans. Graph*, 19(4):279–301, 2000.

[WN01] Geir Westgaard and Horst Nowacki. Construction of fair surfaces over irregular meshes. In *Symposium on Solid Modeling and Applications*, pages 88–98, 2001.

[WP97] Johannes Wallner and Helmut Pottmann. Spline orbifolds. In *Curves and surfaces with applications in CAGD (Chamonix–Mont-Blanc, 1996)*, pages 445–464. Vanderbilt Univ. Press, Nashville, TN, 1997.

[Ye97] Xiuzi Ye. Curvature continuous interpolation of curve meshes. *Computer Aided Geometric Design*, 14(2):169–190, 1997.

[YZ04] Lexing Ying and Denis Zorin. A simple manifold-based construction of surfaces of arbitrary smoothness. *ACM TOG*, 23(3):271–275, August 2004.